Acta Ophthalmologica

Acta Ophthalmologica 2022

Translation model for anterior segment tomographic data to corneal spherical aberration derived from a Monte-Carlo simulation based on raytracing

Achim Langenbucher,[1] Nóra Szentmáry,[2,3] Alan Cayless,[4] Lena Münninghoff,[5] Rosalie Wortmann,[5] Jascha Wendelstein[1,6] and Peter Hoffmann[5]

[1]Department of Experimental Ophthalmology, Saarland University, Homburg/Saar, Germany
[2]Dr. Rolf M. Schwiete Center for Limbal Stem Cell and Aniridia Research, Saarland University, Homburg/Saar, Germany
[3]Department of Ophthalmology, Semmelweis-University, Budapest, Hungary
[4]School of Physical Sciences, The Open University, Milton Keynes, UK
[5]Augen- und Laserklinik Castrop-Rauxel, Castrop-Rauxel, Germany
[6]Medical Faculty, Johannes Kepler University Linz, Linz, Austria

ABSTRACT.

Background: **Intraocular lenses with a negative aspherical design for correction of corneal spherical aberration (SA) have gained popularity in recent decades. In most cases, a 'one size fits all' concept is followed, where all eyes receive lenses with the same SA correction. The purpose of this study is to develop a strategy based on raytracing using anterior segment tomography data to extract corneal SA and to provide simple multivariable linear models for prediction of corneal SA.**

Methods: **The analysis was based on a large dataset of 8737 measurements of 8737 eyes from 1 clinical centre, using the Casia2 anterior segment tomographer. An optical model based on: corneal front and back surface radius Ra and Rp, asphericities Qa and Qp, corneal thickness CCT, anterior chamber depth ACD, and pupil centre position (X-Y position: Pup_X and Pup_Y), was defined for each measurement. Corneal SA was derived using a 6-mm aperture perpendicular to the incident ray and centred on the chief ray, and linear prediction models were derived for SA using biometric data. Cross-validation was used for model performance evaluation.**

Results: **Using raytracing, the wavefront error within an aperture (6-mm diameter centred on the intersection of the chief ray with the cornea) was calculated and corneal SA was extracted. After identifying the relevant effect sizes (Ra, Qa, Rp Qp, ACD, Pup_X and Pup_Y) using stepwise linear regression, linear mixed-effects models (model 1: all effect sizes, model 2: Ra, Qa, Rp and Qp, model 3: Ra and Qa) were set up on the training data in terms of a Monte-Carlo simulation. On the test data (training data), model 1 with a mean absolute/root-mean-squared prediction error of 0.0095/0.0130 (0.0095/0.0127) performed similarly to model 2 with 0.0097/0.0131 (0.0096/0.0127), and both outperformed model3 with 0.0152/0.0197 (0.0148/0.0190).**

Conclusion: **Based on the Casia2 anterior segment tomographer, corneal SA could be derived using shape data (curvature and asphericities) of both corneal surfaces (model 2). This information could easily be used for selection of the appropriate negative aspherical lens design in cataract surgery.**

Key words: cataract surgery – cornea asphericity – linear mixed-effects model – Monte-Carlo simulation – raytracing – spherical aberration

Acta Ophthalmol. 2022: 100: e1665–e1674

doi: 10.1111/aos.15125

Background

Over the last 2 decades aspherical intraocular lenses have gained popularity in cataract surgery as replacements for the opaque crystalline lens. Many different optical designs have been brought to market: in addition to spherical designs with spherical front and back lens surfaces, we have the category of aberration-free or aberration-neutral lenses that are intended not to change overall ocular spherical aberration (SA) (the SA of the pseudophakic eye equals the SA of the aphakic eye). In addition, we have the category of aberration correcting lenses that are intended to reduce or eliminate the SA of the eye by compensating for the SA of the cornea (which shows typically positive values) with a negative SA in the lens (Kohnen & Klaproth 2008; Wang et al. 2012).

The term 'aberration-free' or 'aberration-neutral' in the context of cataract surgery is not clearly defined in the literature: Whereas some lens designs neutralize the intrinsic SA for a collimated entrance beam and show positive SA for a convergent incident ray bundle (*e.g.* located behind a (model) cornea), others neutralize the intrinsic SA for a convergent entrance beam and show negative SA for a

collimated incident ray bundle (Langenbucher et al. 2017). In contrast, aberration correcting lenses always induce some amount of negative SA if located behind a (model) cornea (with an incident convergent beam). Depending on the correction concept, which is mostly based on a schematic model eye, and the amount of SA to be corrected, there are lenses on the market with an SA correction in a range between 0.10 μm and 0.27 μm.

Unlike ocular spherical aberration, corneal spherical aberration cannot be measured directly with any device (Sicam et al. 2006; Calossi 2007; Nochez et al. 2010; Al-Sayyari et al. 2014; De Jong et al. 2016). In place of measurement, corneal SA can be calculated from corneal tomography data, which requires raytracing strategies (Langenbucher et al. 2021). In most tomographers, a conversion from corneal asphericity to corneal spherical aberration is implemented, but the methodology of the conversion, the reference plane, the radius and the centre of the unit circle for the Zernike decomposition, as well as the reference axis are not known/disclosed (Wang & Bao 2017).

The amount of SA correction typically mentioned in the data specification sheet refers to the SA correction at corneal front surface plane referenced to a 6-mm zone. This means that the value provided by the lens manufacturer in terms of a Zernike coefficient (given in a μm scale) is related to a specific environment characterized by a specific location of the lens relative to the cornea and pupil position, where the pupil centre together with the angle of the incident ray bundle defines the visual axis. As this environment is not standardized, lens manufacturers use different lens models for specifying the lens SA, and therefore, the 'real' amount of SA correction in an individual eye may vary (Schrecker et al. 2019).

In current clinical practice, the selection of lens type (spherical or aspherical) according to the corneal SA of the individual eye is rarely considered. (Solomon 2010; Du et al. 2019; Schrecker et al. 2019). Wavefront aberrometers measure the optical aberrations of the entire eye (Atchison et al. 2016), but the result of ocular aberration measurement prior to cataract surgery is not relevant for lens selection, as the crystalline lens with its intrinsic optical aberrations is removed from the optical system. However, in the absence of corneal pathologies, with the new generation of anterior segment tomographers, many clinically relevant parameters, including the curvature of the corneal front and back surface and asphericity, and the central corneal thickness can be measured quite precisely. In cases of corneal pathologies such as tear film insufficiency, ectatic diseases such as keratoconus, keratoglobus or pellucide marginal degeneration, or with fixation instabilities, the variability of the measurement parameters may however increase significantly.

A Cartesian coordinate system is typically defined with its origin at the corneal front apex with axial direction Z towards the retina and lateral directions X (horizontal axis, positive values to the right) and Y (vertical direction, positive values up). In addition, there are measurement data for the axial and lateral position of the pupil centre and the pupil diameter. From these data, the corneal SA value for a 6-mm zone at corneal front apex plane can be derived using raytracing techniques. With this value and the general definition of the amount of SA correction value from the lens data sheet, clinicians can select the appropriate lens model to compensate for the individual corneal SA (Schrecker et al. 2019).

The purpose of this study is (i) to provide a calculation strategy for extracting the corneal SA value referenced to a 6-mm zone at the corneal apex plane from measurement data of a clinically established high-resolution anterior segment OCT in a very large dataset based on raytracing techniques, (ii) to identify the relevant effect sizes and (iii) to model the results with a linear mixed-effects model in terms of a Monte-Carlo simulation. The resulting spherical aberration value from the model could be directly used together with the nominal SA correction from the lens data sheet to estimate the spherical aberration of the pseudophakic eye after cataract surgery.

Methods

Dataset for the Monte-Carlo simulation

In total, a dataset with 11 277 measurements from one clinical centre (Augenklinik Castrop-Rauxel, Germany) taken using the Casia2 anterior segment tomographer (Tomey, Nagoya, Japan) was considered for this retrospective study. Duplicate measurements of eyes and incomplete data in the dataset were discarded. Measurements from pseudophakic eyes or in mydriasis and data indexed with situation after refractive surgery, ectatic corneal diseases or other corneal pathologies were excluded from the dataset. The data were transferred to a.csv data table using the data export module of the Casia2 software. Data tables were reduced to the relevant parameters required for our raytracing and analysis, consisting of patient ID, laterality (left or right eye), central corneal curvature of the corneal front (Ra) and back (Rp) surface in mm, asphericity of the corneal front (Qa) and back (Qp) surface, central corneal thickness (CCT in mm), anterior chamber depth (ACD) measured from the corneal front apex to the lens front apex in mm, pupil size (Pup) in mm, as well as the location of the pupil centre (Pup_X in horizontal and Pup_Y in vertical direction), both in mm. The data were transferred to Matlab (Matlab 2019b, MathWorks, Natick, USA) for further processing. The study was registered with the local Ethics committee (Ärztekammer des Saarlandes, 157/21).

Preprocessing of the data and raytracing

Custom software was written in Matlab. By convention we defined a Cartesian coordinate system with its origin at the corneal front apex, X axis to the right, Y axis in the superior direction, and Z axis towards the retina. The optical model is represented by a structure consisting of a cornea with 2 coaxial aspheric surfaces defined by Ra, Qa, Rp, Qp and CCT. Accordingly, the coordinates of the elements in the optical model were X/Y/Z = 0/0/0 for the corneal front apex, 0/0/CCT for the corneal back apex and Pup_X/Pup_Y/ACD for the pupil centre (decentration Pup_X in horizontal and Pup_Y in vertical direction) respectively. For air/cornea/aqueous humour, we used refractive index values of 1.0/1.376/1.336, respectively, taken from the Liou-Brennan schematic model eye (Liou & Brennan 1997). Without loss of generality, in order to consider all samples as left eyes, the optical model was flipped horizontally for right eyes, which means that the sign for Pup_X

was changed keeping Pup_Y unchanged. Positive values for X and Y refer to the temporal and superior direction.

As the incident ray angle with components I_X/I_Y cannot be measured and therefore we do not have normative values, we used for the mean value the data from the Liou-Brennan schematic model eye (mean of $I_X = 5°$ from nasally, mean of $I_Y = 0°$). For right eyes, the sign of the I_X component was flipped. Additionally, we added a normal distribution with a standard deviation of 2° and finally discarded values outside the range [−9° to −1° / −4° to 4°] for I_X/I_Y. Using this strategy, we considered the eccentric location of the fovea shifted in the temporal direction (positive values of X).

The entire dataset was split into training data (70%) and test data (30%) for a hold-out cross-validation strategy. The training data were used for extracting the relevant effect sizes and building up the model, and the performance of the prediction model was subsequently evaluated with the test data.

Calculating the SA

For initialization, a parametric ray with an incident ray angle I_X/I_Y and variable offset in X and Y direction was projected onto the corneal front apex and traced through both corneal surfaces to the pupillary plane. The distance of the ray–pupil intersection was extracted, and using an iterative nonlinear optimisation strategy (Interior Point Method (IPM), Karmarkar 1984), the ray was shifted in X and Y to pass through the pupil centre (chief ray). The coordinates of the intersection of the chief ray with the corneal front surface plane were calculated as X_0/Y_0. In the next step, a circular aperture with a diameter of 6 mm was defined centred on X_0/Y_0 and perpendicular to the incident-collimated ray. This new aperture is tilted by I_X/I_Y to the optical axis (Z direction of the Cartesian coordinate system) in order to be aligned to the incident ray (or the fixation axis of the patient). After removing the initial pupil from the optical system (located with its centre at X/Y/Z = ACD, Pup_X, Pup_Y) a bundle of collimated rays (20 000 equidistant rays) with a diameter of 7 mm was traced through the optical system consisting of an aperture, the corneal front surface and the corneal back surface, and the best wavefront focus was identified by minimizing the root-mean-squared wavefront error. The optical path lengths were calculated from the source to the best wavefront focus. For all rays passing through the 6-mm aperture at X_0/Y_0, the optical path length differences were derived with respect to the aperture plane. For that purpose, all coordinates of the ray intersections with a plane Z = 0 were calculated, and the X /Y /Z coordinates were back-rotated by Euler angles $-I_X/-I_Y$ to extract the wavefront with respect to the plane perpendicular to the collimated incident ray. This rotation was performed using quaternion transformation (St. Pierre 2021). Finally, a Zernike decomposition of all optical path length differences within the aperture (3-mm radius of the unit circle) was performed, and the Zernike coefficient Z_4^0 was extracted representing the spherical aberration of the cornea independent from the pupil size measured with the Casia2. Figure 1 shows an example for 10 000 rays and model data derived from the Liou-Brennan schematic model eye (Ra/Qa/Rp/Qp/CCT/ACD/Pup_X/Pup_Y/I_X/I_Y = 7.77 mm/−0.18/6.4 mm/−0.6/0.5 mm/3.66 mm/−0.5 mm/0.0 mm/−5°/0°) the characteristics of the wavefront error (optical path length differences) in a plane perpendicular to the ray bundle together with the unit circle (6 mm in diameter, red circle) on which the Zernike coefficients were based. The resulting SA value was 0.27 µm.

Identifying the relevant effect sizes for the multilinear regression model

A stepwise linear regression (Draper & Smith 1998) was implemented to analyse the relevant effect sizes for a multilinear prediction model for the target parameter SA from the potential input parameters Ra, Qa, Rp, Qp, CCT, ACD, Pup_X, Pup_Y, I_X and I_Y. This stepwise algorithm was applied to the training data, with the test data excluded. The stepwise strategy begins with an initial constant model and takes forward and backward steps to add or remove variables, until a stopping criterion is satisfied. As stopping criteria, we restricted the number of iterations to a maximum of 100, iteration steps smaller than 10e-9 or improvement of the root-mean-squared prediction error by less than 10e-12. The tolerance for adding terms was a significance value less than 0.05, and the tolerance for removing terms was a significance value larger equal 0.05.

Setup of a multivariable linear prediction model

With the effect sizes identified from this stepwise fit, a linear mixed-effects model (Herber et al. 2020) based on the training data was set up to predict the corneal SA. The biometric parameters were used as fixed effects, whereas the patient ID was considered as a grouping variable (random effects) in order to consider the effect of correlation between both eyes of an individual (Herber et al. 2020). In addition, a simplified linear mixed-effects model restricted to corneal front surface measurement data available from corneal topography was defined. These prediction models were applied to the test data for cross-validation in order to obtain a readout of the performance characteristics.

Statistical analysis

For explorative data analysis of the input and output (SA) data, we provided the mean (MEAN) and standard deviation (SD), median value (MEDIAN), as well as 90% confidence interval (lower boundary: 5% quantile and upper boundary: 95% quantile), and 99% confidence interval (lower boundary: 0.5% quantile and upper boundary: 99.5% quantile). The performance of the prediction models derived from the training data were analysed using the test data with scatterplots displaying the modelled SA data versus the observed SA data from raytracing. The model prediction error PE was considered as the deviation of the multivariable linear model output minus the observed SA from raytracing. The performance of the model was expressed using the correlation coefficient R, significance level P (comparing the actual model against a constant model), the lower and upper boundaries of the 95% confidence interval for R (R_{LO} and R_{UP}), the mean prediction error (meanPE), the mean absolute prediction error (meanABSPE) and the root-mean-squared prediction error (rmsPE).

Results

After quality approval of the dataset and filtering out incomplete data, a final total of N = 8737 measurements (4232 right and 4505 left eyes from 5188 patients) were used for our Monte-Carlo simulation. The process time for extracting the chief ray passing through the pupil centre and tracing 20 000 rays through the 8737 optical models including extraction of the SA

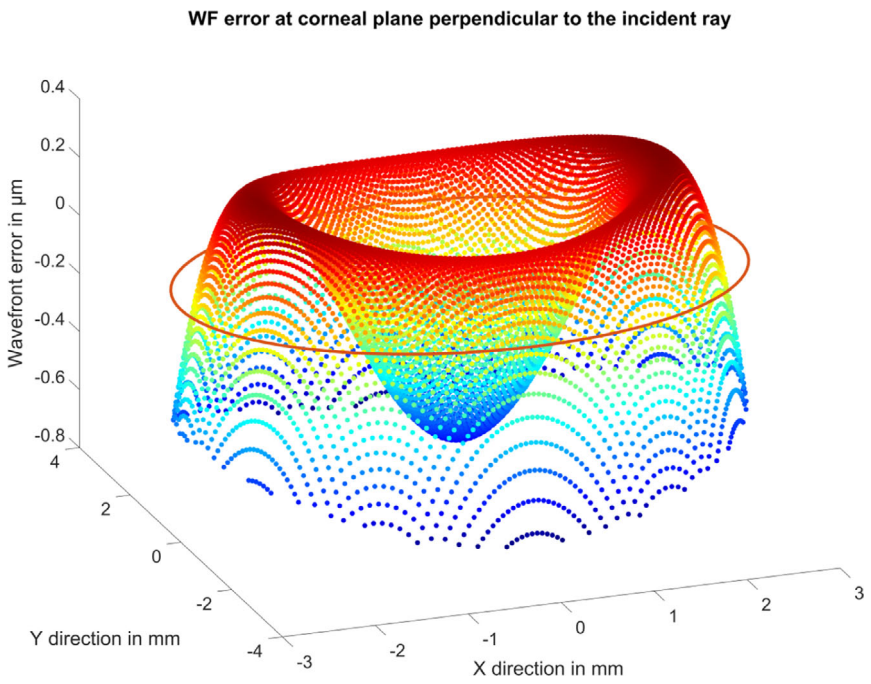

Fig. 1. Example of a wavefront (WF) error (optical pathlength differences) extracted from raytracing through model data derived from the Liou-Brennan schematic model eye. For this simulation with 10 000 equidistant rays we used (Ra/Qa/Rp/Qp/CCT/ACD/Pup_X/Pup_Y/I_X/I_Y = 7.77 mm/−0.18/6.4 mm/−0.6/0.5 mm/3.66 mm/−0.5 mm/0.0 mm/−5°/0°). After identifying the chief ray passing through the pupil centre, the pupil was removed and a new aperture with a 6-mm diameter was defined perpendicular to the incident ray and centred on the intersection of the chief ray with the corneal front surface. The reference unit circle for the Zernike decomposition with a 6-mm diameter is shown as a red line.

value took 24 733 seconds (6 hours 52 min) on a standard office PC. Table 1 shows the explorative data for Ra, Qa, Rp, Qp, CCT, ACD, Pup (not used for calculating corneal SA), the pupil centre position Pup_X and Pup_Y derived from the Casia2 anterior segment OCT in horizontal and vertical direction, the incident ray angles I_X and I_Y in horizontal and vertical direction, as well as the corneal spherical aberration SA (Z_4^0). The wavefront error was considered within a 6-mm zone at a plane perpendicular to the incident-collimated beam centred on the intersection of the chief ray with the corneal front surface. The horizontal position of the pupil centre Pup_X and the horizontal incident ray angle I_X were flipped in sign for right eyes to simulate left eyes only, meaning that positive values for X and Y refer to the temporal and superior directions respectively. The dataset was split randomly into training data (N = 6116, 70%) and test data (N = 2621, 30%).

Figure 2 shows the scatterplot matrix for the input parameters RA, Qa, RP, Qp, CCT, ACD, Pup_X, Pup_Y, I_X, I_Y, and the output parameter SA, separately for left eyes (in green) and right eyes (in red) before flipping the sign of horizontal pupil position and horizontal incident ray angle of left eye data. The respective histograms are plotted on the diagonal of the matrix. From the scatterplot matrix, it can be seen that left eyes and right eyes show similar behaviour in Ra, Qa, Rp, Qp, CCT, ACD, Pup_Y, I_Y and SA. The distributions of Pup_X and I_X are mostly symmetrical about the Y axis (flipped in sign). The most important effect size for corneal SA appears to be the asphericity value of the corneal front surface Qa.

Figure 3 displays the cumulative density function (CDF) of corneal SA extracted from the wavefront error considered in a 6-mm zone (unit circle) at a plane perpendicular to the incident rays. In the plot, we have added the benchmarks of the 90% and 99% confidence intervals shown as red and blue lines. From the graph, it can be seen that the SA value shows a mostly symmetrical distribution.

To investigate the relevant effect sizes, we used the following parameters as potential input values for our stepwise linear regression: Ra, Qa, Rp. Qp. CCT, ACD, Pup_X and Pup_Y. In our final optical model for extracting corneal SA, we used a circular aperture with a 6-mm diameter centred on the intersection of the chief ray (passing through the pupil centre) with the corneal front surface oriented perpendicularly to the incident ray. Therefore, the pupil size measured with the Casia2 (Pup) was not considered for our model. As the incident ray angle was synthesized using a random generator, we decided to discard the parameters I_X and I_Y from the modelling. The stepwise fit algorithm that qualifies the input parameters for our linear multivariable prediction model based on the training data showed convergence after 7 iterations. As relevant effect sizes, we identified the parameters Ra, Qa, Rp, Qp, ACD, Pup_X and Pup_Y.

Model 1: For the parameters identified as relevant effect sizes, we set up a linear mixed-effects model based on the training data considering the patient ID as a grouping variable which reads:

$$\begin{aligned} SA = {} & 0.9262 - 0.0935 \bullet R_a \\ & + 0.7154 \bullet Q_a + 0.0223 \bullet R_p \\ & - 0.1219 \bullet Q_p - 0.0026 \bullet ACD \\ & + 0.0062 \bullet Pup_X - 0.002 \bullet Pup_Y \end{aligned}$$

The respective standard errors P values for the intercept and the 7 regression coefficients Ra, Qa, Rp, Qp, ACD, Pup_X, Pup_Y mentioned above are 0.0048/<1e-100, 0.0008/<1e-100, 0.0013/<1e-100, 0.0010/<1e-100, 0.0014/<1e-100,

Table 1. Explorative data extracted from the dataset of the Casia2 anterior segment tomograph. Ra, Qa, Rp, Qp, CCT, ACD, Pup, Pup_X, Pup_Y, I_X, I_Y refer to the corneal front surface curvature and asphericity, corneal back surface curvature and asphericity, central corneal thickness, anterior chamber depth measured from the corneal front apex, pupil diameter Pup, lateral position of the pupil centre in X (positive values in the temporal direction) and Y (positive values in the superior direction), and simulated incident ray angle in X and Y. Right eyes were flipped in X. MEAN, SD, MEDIAN refer to mean value, standard deviation and median, and 5% quantile/95% quantile and 0.5% quantile/99.5% quantile to the lower and upper boundaries of the 90% and 99% confidence intervals respectively.

N = 8737	Ra in mm	Qa	Rp in mm	Qp	CCT in mm	ACD in mm	Pup in mm	PupX in mm	PupY in mm	I_X in °	I_Y in °	SA
MEAN	7.76	−0.23	6.56	−0.11	0.55	3.36	3.32	−0.31	−0.10	−5.02	0.01	0.19
SD	0.28	0.13	0.25	0.11	0.04	0.40	0.81	0.21	0.18	1.73	1.46	0.09
MEDIAN	7.74	−0.22	6.56	−0.10	0.55	3.37	3.31	−0.30	−0.10	−5.01	0.01	0.19
5% quantile	7.33	−0.45	6.17	−0.34	0.49	2.67	2.45	−0.60	−0.40	−7.94	−2.44	0.03
95% quantile	8.27	−0.02	6.99	0.06	0.60	3.99	4.66	0.00	0.20	−2.14	2.41	0.34
0.5% quantile	7.13	−0.49	5.99	−0.46	0.42	2.30	2.21	−0.90	−0.60	−8.80	−2.93	−0.01
99.5% quantile	8.79	0.08	7.26	0.10	0.64	4.37	4.95	0.30	0.40	−1.26	2.92	0.44

0.0004/1.20e-9, 0.0008/5.74e-14 and 0.0008/0.0203 respectively.

Applying this model to the training data/test data yields the performance data as shown in the upper part of Table 2. The respective performance plot where the modelled corneal SA is displayed versus the SA derived from raytracing is shown in the upper graph of Fig. 4.

Model 2: In addition, a simplified prediction model was set up based on the training data with the parameters Ra, Qa, Rp, Qp:

$$SA = 0.9180 - 0.0939 \cdot R_a + 0.7154 \cdot Q_a + 0.0224 \cdot R_p - 0.1222 \cdot Q_p$$

The respective standard errors P values for the intercept and the 4 regression coefficients mentioned above are 0.0046/<1e-100, 0.0009/<1e-100, 0.0013/<1e-100, 0.0010/1.02e-79 and 0.0014/<1e-100 respectively.

Applying this model to the training data/test data yields the performance data as shown in the middle part of Table 2. The respective performance plot where the modelled corneal SA is displayed versus the SA derived from raytracing is shown in the middle graph of Fig. 4.

Model 3: Furthermore, a sparse prediction model was set up based on the training data with the parameters Ra, Qa only, which could be derived also from corneal front surface corneal topography:

$$SA = 0.9622 - 0.0791 \cdot R_a + 0.7069 \cdot Q_a$$

The respective standard errors P values for the intercept and the 2 regression coefficients mentioned above are 0.0067/<1e-100, 0.0009/<1e-100 and 0.0019/<1e-100 respectively.

Applying this model to the training data/test data yields the performance data as shown in the lower part of Table 2. The respective performance plot where the modelled corneal SA is displayed versus the SA derived from raytracing is shown in the lower graph of Fig. 4.

Discussion

In recent decades, many different concepts for aspherical intraocular lenses have been developed (Kohnen & Klaproth 2008; Wang et al. 2012). Currently, we have so called aberration-neutral or aberration-free lens designs having a slightly negative aspherical base curve, as well as aberration correcting lenses with some higher amount of negative asphericity at one or both optical surfaces (Langenbucher et al. 2017). However, to date, the philosophy behind aspherical lenses has been a 'one size fits all' strategy, and therefore, all lens types on the market have one specific amount of correction for the spherical aberration (Wang et al. 2012). This value for the SA correction, which by convention refers to the Zernike term Z_4^0, is provided by convention with respect to the corneal front surface plane and a 6-mm zone (diameter of the unit circle for the Zernike decomposition). However, the effect of spherical aberration within an individual eye may be different, as the conversion of the SA correction from lens plane to the corneal plane is affected by the incident ray and several biometric parameters (*e.g.* corneal curvature or axial position of the lens with respect to the cornea). Therefore, this conversion is mostly specified with respect to a certain schematic model eye, but the lens manufacturers normally do not provide information on which parameter set or which model eye was used for this conversion.

Based on the assumption that the amount of SA correction provided in the data sheet of the lens is correct for our individual patient, we could apply raytracing techniques to find out the amount of corneal SA at the same reference plane and the same reference zone where we have data on the SA correction of the lens. In this case, we could simply add up the corneal SA (Langenbucher et al. 2017) as obtained from raytracing and the SA correction provided by the lens manufacturer to estimate the resulting SA (at corneal plane) in the pseudophakic eye after cataract surgery. However, we have to keep in mind that spherical aberration of the eye also enlarges the depth of focus, which could support near vision. Therefore, many intraocular lens manufacturers do not provide aspherical lenses, which are designed to fully correct the spherical aberration (of a schematic model eye).

The concept for extracting corneal SA from tomographic data is simple: we construct an optical model based on measurement data from an anterior segment tomographer using the shape of the corneal front and back surface, central corneal thickness, anterior chamber depth and the location of the pupil centre. Assuming that the axial location of the pupil is in the plane of the anterior lens surface, only the direction of collimated incident ray is required as a

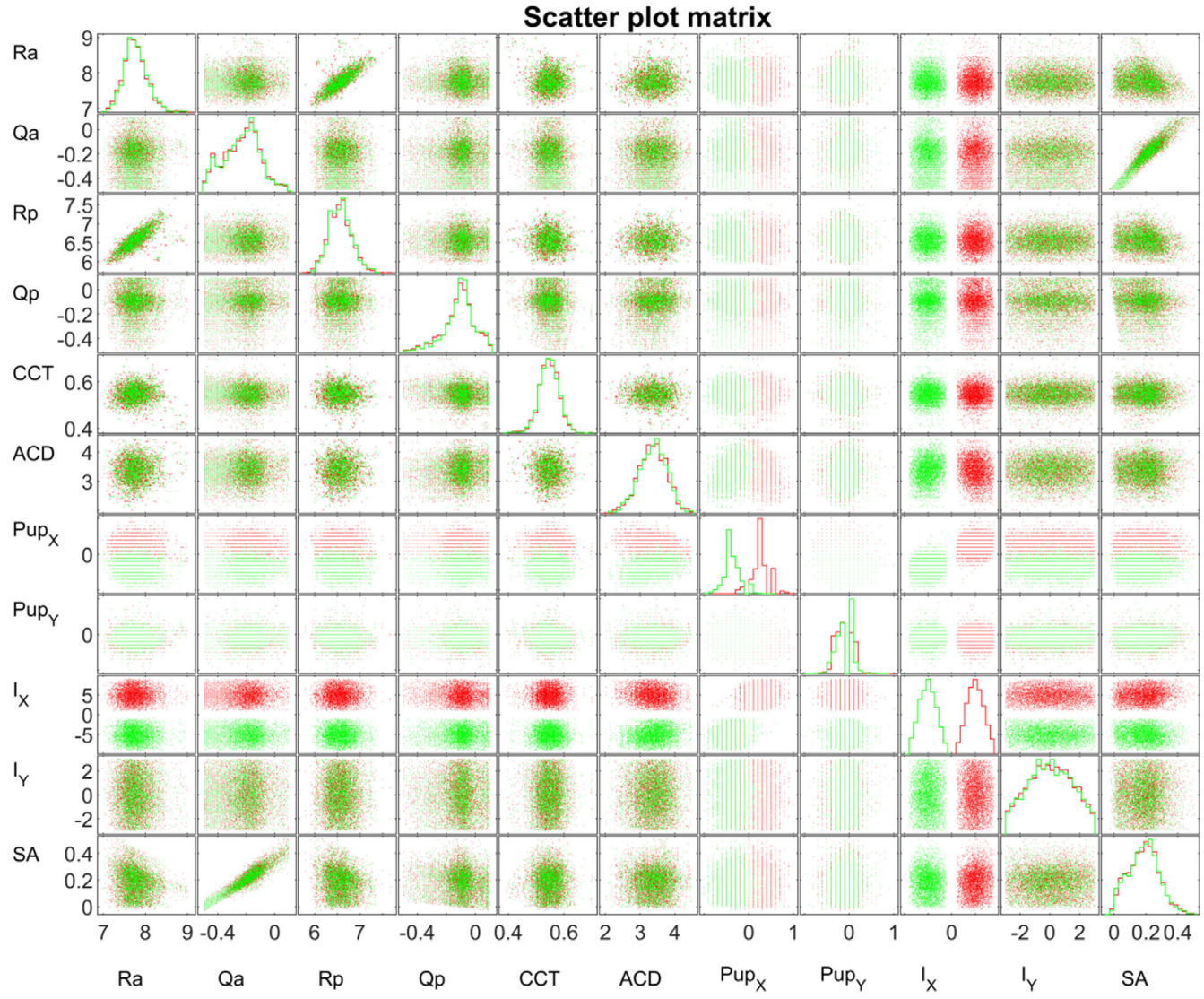

Fig. 2. Matrix of grouped scatterplots for the potential input parameters of the multivariable linear prediction model (Ra/Qa/Rp/Qp/CCT/ACD/Pup_X/Pup_Y/I_X/I_Y) and the spherical aberration SA calculated from the Zernike decomposition of the wavefront error considered in a plane perpendicular to the incident ray with a 6-mm diameter. Left eyes/right eyes are plotted in green/red. Please note that for this graph, left eyes were not flipped horizontally. The respective histograms are plotted on the diagonal of the matrix. From the graph, it is obvious that the corneal front surface asphericity is the most relevant effect size for SA.

missing link. For simplification, we assume that all refractive surfaces in the eye are coaxially aligned, that only the pupil centre may be decentred and that the incident ray may be oblique. In this simplification, the 'optical axis' of the system is defined by all the coaxial refractive surfaces, and the incident ray describes the angle alpha, which in general cannot be measured with any instrumentation. In the present study, we used a random value for the incident ray angle with a mean of −5/5 degree for left/right eyes and a standard deviation of ±2° for both directions. As the angle alpha cannot be measured, we decided to omit I_X and I_Y from the prediction models. However, as can be seen from our performance plots, the variation between the corneal SA derived from raytracing and the corneal SA derived from the 3 linear mixed-effects models is quite good, meaning that the incident ray angle may not only have a major impact on the tilt terms (Z_1^1 and Z_1^{-1} of the wavefront), but only a minor effect on the SA term Z_4^0. Therefore, we feel that information on the visual axis is not mandatory for estimating the corneal SA from the tomographic data. As an alternative, we could use information from the Chang-Waring chord as offset between the Purkinje light reflex PI and the pupil centre to retrieve data on the visual axis (Chang & Waring 2014; Holladay 2019; Jiang et al. 2020) in order to predict the incident ray angle from tomography.

Using a large dataset derived from the high-resolution anterior segment OCT Casia 2 from one clinical centre, we implemented a raytracing concept to calculate the optical path length differences in terms of a wavefront analysis. As the instrument axis is oriented coaxially with the incident beam, the optical pathlength dfferences had to be considered with respect to a plane perpendicular to the incident beam. Therefore, the reference plane considered for the wavefront analysis was tilted using a quaternion transformation with Euler angles as shown in the literature (St. Pierre 2021).

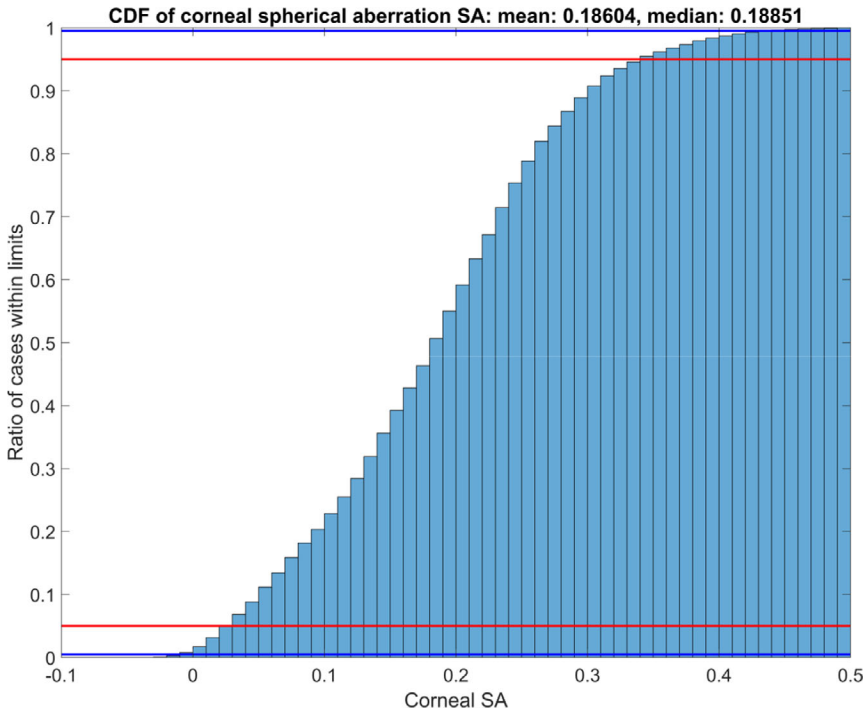

Fig. 3. Cumulative distribution function of the spherical aberration SA derived from raytracing through $N = 8737$ eyes. Corneal SA was extracted from the wavefront error using a Zernike decomposition considered at a plane perpendicular to the incident ray (within a 6-mm zone defined as unit circle). In the plot, we have added the lower and upper boundaries of the 90% (red lines) and 99% (blue lines) confidence intervals.

Table 2. Performance of the 3 linear mixed-effects models (with patient ID as a grouping variable) derived from the training data. The models were applied to the training data and to the test data in a cross-validation process to check for potential overfitting. In this table, we provide the correlation coefficients R with the lower and upper limits of the confidence intervals R_{LO} and R_{UP}, the significance level comparing the model to a constant model (P), together with the mean prediction error (meanPE), the mean absolute prediction error (meanABSPE) and the root-mean-squared prediction error (rmsPE). There is no relevant difference in the performance data when applying the prediction model to the training data or to the test data, confirming that we do not have overfitting in the models.

$N = 8737$	R	p	R_{LO}	R_{UP}	meanPE	meanABSPE	rmsPE
Prediction model based on Ra, Qa, Rp, Qp, CCT, Pup_X, Pup_Y							
Training data $N = 6116$	0.9910	<1e-100	0.9906	0.9915	0.0000	0.0095	0.0127
Test data $N = 2621$	0.9907	<1e-100	0.9899	0.9914	−0.0001	0.0095	0.0130
Simplified prediction model based on Ra, Qa, Rp, Qp							
Training data $N = 6116$	0.9909	<1e-100	0.9904	0.9913	0.0000	0.0096	0.0127
Test data $N = 2621$	0.9905	<1e-100	0.9898	0.9911	−0.0001	0.0097	0.0131
Sparse prediction model based on Ra, Qa only							
Training data $N = 6116$	0.9797	<1e-100	0.9786	0.9807	0.0000	0.0148	0.0190
Test data $N = 2621$	0.9785	<1e-100	0.9768	0.9800	0.0005	0.0152	0.0197

Finally, the resulting wavefront error was decomposed into Zernike terms with a unit circle diameter of 6 mm to obtain the corneal SA term. The corneal SA was then modelled with a linear mixed-effects model (Herber et al. 2020). Linear mixed-effects models were used instead of standard linear models to consider the effect of intrapatient correlations in the dataset. To obtain realistic values for the model performance, we split our dataset into training and test data for cross-validation (hold-out strategy) using typical proportions of 70% for the training data and 30% for the test data. The models were trained using the training data and then validated using the test data. In addition, the models were also applied to the training data for a comparison of the performance characteristics with the respective performance data as applied to the test data. In our case, the performance of the model as applied to the test and the training data are quite similar as shown in Table 2, confirming that overfitting was not encountered in any of our prediction models. For Model 1, we used all of the parameters identified as effect sizes by our stepwise regression algorithm (Ra, Qa, Rp, Qp, CCT, Pup_X and Pup_Y). In addition, we restricted the model to a simplified model (Model 2), which considers only the shape data of the corneal front and back surface and ignores central corneal thickness CCT and the location of the pupil centre Pup_X and Pup_Y. Finally, we simplified again to a sparse model (Model 3), which considers only the corneal front surface shape with Ra and Qa. This sparse

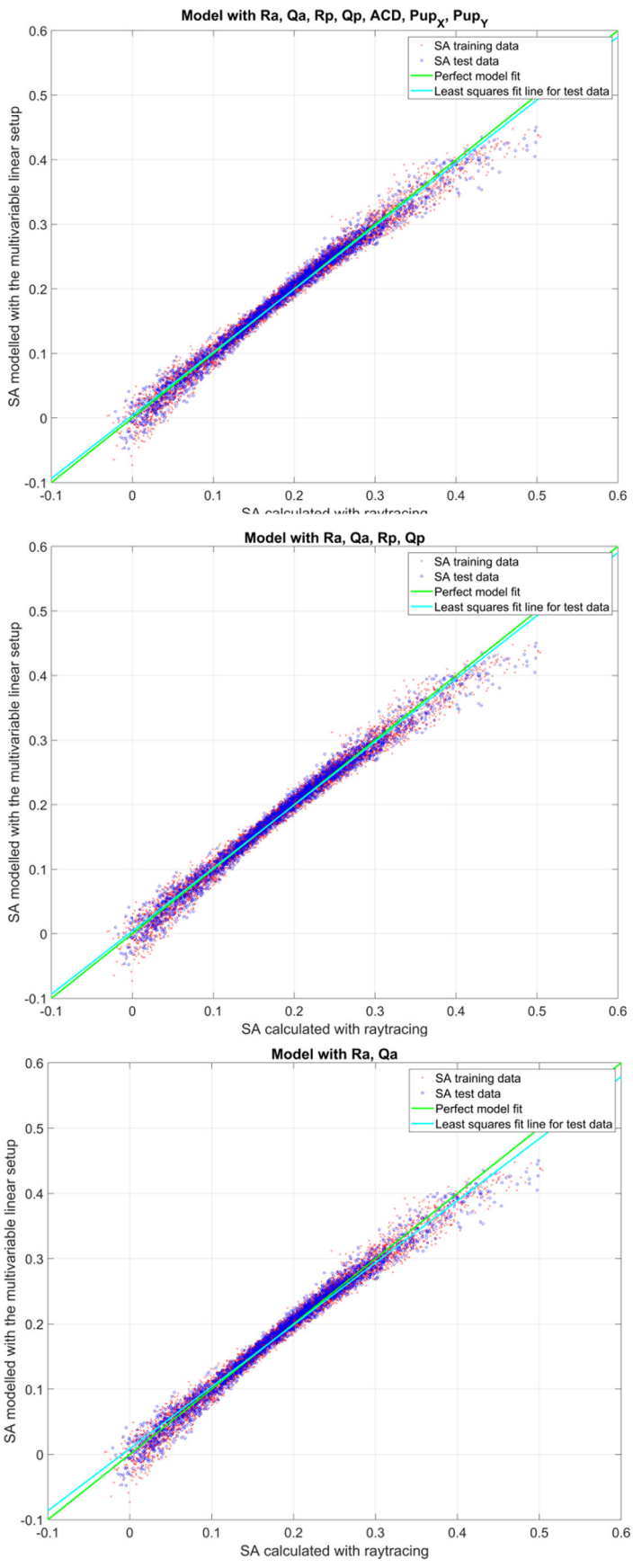

Fig. 4. Performance of the three linear models: In the upper graph, the corneal SA from the linear prediction model using Ra, Qa, Rp, Qp, ACD, Pup_X and Pup_Y is plotted versus the corneal SA derived from raytracing; in the middle graph, the corneal SA from the linear prediction model using Ra, Qa, Rp and Qp is plotted versus the corneal SA derived from raytracing; in the lower graph, the corneal SA from the linear prediction model using Ra, Qa is plotted versus the corneal SA derived from raytracing. In all three graphs, we have included the line for a perfect model fit (where the corneal SA from the prediction model fits the SA from raytracing, green line) as well as a least-squares fit line (cyan line, only shown for the test data).

model could also be used where measurement data are only available for the corneal front surface (*e.g.* from corneal topography), and not for the corneal back surface shape or central corneal thickness. Overall, we feel that all 3 linear prediction models perform well in predicting corneal SA from measurement data of the Casia2 anterior segment analyser. As can be seen from Table 2, there is not too much difference between Model 1 and Model 2, but both models slightly outperform the sparse model (Model 3) in terms of mean absolute prediction error (meanABSPE) and root-mean-squared prediction error (rmsPE). The respective performance plots for the initial model, the simplified model and the sparse model are shown in Fig. 4. Here, the modelled corneal SA is displayed versus the corneal SA derived from raytracing together with the least-squares linear regression line.

There are some limitations in our study: we restricted the model to a simple optical model for the cornea with rotationally symmetric aspherical surfaces aligned on a common axis (which was considered as the 'optical axis'). Additionally, we ignored the effect that the location of the pupil centre is affected by the pupil size as shown by Erdem et al. (2008); Yang et al. (2002). According to the convention of reporting the amount of SA correction with a 6-mm optical zone at corneal plane, we restricted our raytracing setup to this scenario. In the future, different optical zones could be used to investigate the effect of corneal spherical aberration as a function of pupil size. Further, there were no measurement data of the incident ray angle, and therefore, we had to use random data in our simulation instead based on mean values ($I_X = -5°$ / $I_Y = 0°$ for left eyes) from a modern schematic model eye (Liou & Brennan 1997), and last but not least, there are only limited data about the quality of the corneal asphericity measurements, about the characteristics in a cataractous population (De Sanctis et al. 2014) and especially about long-term changes (Amorim-de-Sousa et al. 2019) or iatrogenic changes due to cataract surgery (Li et al. 2012).

In conclusion, in this paper, we have developed simple linear prediction models to estimate corneal spherical aberration to be used for selecting the appropriate intraocular lens model in cataract surgery. A raytracing strategy was set up to derive corneal spherical aberration from a Zernike decomposition of the wavefront error considered at corneal plane perpendicularly to the incident ray. Our concept is based on a Monte-Carlo simulation with a large dataset from the anterior segment OCT. With cross-validation, the models showed a good performance with all relevant effect sizes identified by a stepwise regression, with a simplified prediction model considering the corneal front and back surface shape, but the performance was slightly lower with a sparse model considering only shape data of the corneal front surface.

References

Al-Sayyari TM, Fawzy SM & Al-Saleh AA (2014): Corneal spherical aberration and its impact on choosing an intraocular lens for cataract surgery. Saudi J Ophthalmol **28**: 274–280.

Amorim-de-Sousa A, Vieira AC, González-Méijome JM & Queirós A (2019): Age-related variations in corneal asphericity and long-term changes. Eye Contact Lens **45**: 99–104.

Atchison DA, Suheimat M, Mathur A, Lister LJ & Rozema J (2016): Anterior corneal, posterior corneal, and lenticular contributions to ocular aberrations. Invest Ophthalmol Vis Sci **57**: 5263–5270.

Calossi A (2007): Corneal asphericity and spherical aberration. J Refract Surg **23**: 505–514.

Chang DH & Waring GO 4th (2014): The subject-fixated coaxially sighted corneal light reflex: a clinical marker for centration of refractive treatments and devices. Am J Ophthalmol **158**: 863–874.

De Jong T, Canovas C, Weeber H & Jansonius NM (2016): From corneal shape to ocular wavefront in eyes with aspheric IOLs: the feasibility of IOL customisation. Ophthalmic Physiol Opt **36**: 43–50.

De Sanctis U, Vinai L, Bartoli E, Donna P & Grignolo F (2014): Total spherical aberration of the cornea in patients with cataract. Optom Vis Sci **91**: 1251–1258.

Draper NR & Smith H (1998): Applied regression analysis. In: Draper NR & Smith H (eds). Probability and statistics, 3rd edn. Hoboken, NJ: Wiley.

Du W, Lou W & Wu Q (2019): Personalized aspheric intraocular lens implantation based on corneal spherical aberration: a review. Int J Ophthalmol **12**: 1788–1792.

Erdem U, Muftuoglu O, Gündogan FC, Sobaci G & Bayer A (2008): Pupil center shift relative to the coaxially sighted corneal light reflex under natural and pharmacologically dilated conditions. J Refract Surg **24**: 530–538.

Herber R, Kaiser A, Grählert X, Range U, Raiskup F, Pillunat LE & Spörl E (2020): Statistische Auswertung korrelierter Messdaten in der Augenheilkunde : Tutorial zur Verwendung des linear gemischten Modells in SPSS und R anhand biomechanischer Parameter der Hornhaut [Statistical analysis of correlated measurement data in ophthalmology : Tutorial for the application of the linear mixed model in SPSS and R using corneal biomechanical parameters]. Ophthalmologe **117**: 27–35.

Holladay JT (2019): Apparent chord mu and actual chord mu and their clinical value. J Cataract Refract Surg **45**: 1198–1199.

Jiang JY, Hodge C & Lawless M (2020): Understanding chord mu through a large population-based study. Clin Exp Ophthalmol **48**: 998–1001.

Karmarkar N (1984) A new polynomial-time algorithm for linear programming. Proceedings of the sixteenth annual ACM symposium on theory of computing – STOC '84. p. 302. doi: https://doi.org/10.1145/800057.808695

Kohnen T & Klaproth OK (2008): Asphärische intraokularlinsen [Aspheric intraocular lenses]. Ophthalmologe **105**: 234–240.

Langenbucher A, Schröder S, Cayless A & Eppig T (2017): Aberration-free intraocular lenses - What does this really mean? Z Med Phys **27**: 255–259.

Langenbucher A, Szentmáry N, Weisensee J, Wendelstein J, Cayless A, Menapace R & Hoffmann P (2021): Prediction model for best focus, power, and spherical aberration of the cornea: raytracing on a large dataset of OCT data. PLoS ONE **16**: e0247048. https://doi.org/10.1371/journal.pone.0247048.

Li ZH, Jia LX & Huang YF (2012): Analysis of corneal spherical aberration in patients before and after phacoemulsification. Eye Sci **27**: 165–168, 172.

Liou HL & Brennan NA (1997): Anatomically accurate, finite model eye for optical modeling. J Opt Soc Am A Opt Image Sci Vis **14**: 1684–1695.

Nochez Y, Favard A, Majzoub S & Pisella PJ (2010): Measurement of corneal aberrations for customisation of intraocular lens asphericity: impact on quality of vision after

micro-incision cataract surgery. Br J Ophthalmol **94**: 440–444.

Schrecker J, Schröder S, Langenbucher A, Seitz B & Eppig T (2019): Individually customized IOL versus standard spherical aberration-correcting IOL. J Refract Surg **35**: 565–574.

Sicam VA, Dubbelman M & van der Heijde RG (2006): Spherical aberration of the anterior and posterior surfaces of the human cornea. J Opt Soc Am A Opt Image Sci Vis **23**: 544–549.

Solomon JD (2010): Outcomes of corneal spherical aberration-guided cataract surgery measured by the OPD-scan. J Refract Surg **26**: 863–869.

St. Pierre J (2021). Quaternion Toolbox. MATLAB Central File Exchange. Available at: https://www.mathworks.com/matlabcentral/fileexchange/1176-quaternion-toolbox. (Accessed on 3 Oct 2021).

Wang L, Canovas C, Weeber HA, Piers PA & Koch DD (2012): Aspheric intraocular lenses. Ophthalmology **119**: 1284.

Wang XJ & Bao YZ (2017): Correlation between axial length and corneal curvature and spherical aberration. Zhonghua Yan Ke Za Zhi **53**: 255–259.

Yang Y, Thompson K & Burns SA (2002): Pupil location under mesopic, photopic, and pharmacologically dilated conditions. Invest Ophthalmol Vis Sci **43**: 2508–2512.

Received on December 14th, 2021.
Accepted on February 18th, 2022.

Correspondence:
Achim Langenbucher
Department of Experimental Ophthalmology
Saarland University
Kirrberger Str 100 Bldg. 22
66424 Homburg
Germany
Tel: +49 6841 1621218
Fax: +49 6841 1621240
Email: achim.langenbucher@uks.eu